buildings

MDPI

Article

Load–Displacement Behaviour and a Parametric Study of Hybrid Rubberised Concrete Double-Skin Tubular Columns

Shovona Khusru [1], David P. Thambiratnam [1], Mohamed Elchalakani [2] and Sabrina Fawzia [1,*]

[1] School of Civil and Environmental Engineering, Faculty of Engineering, Queensland University of Technology, Brisbane 4000, Australia; shovona.khusru@connect.qut.edu.au (S.K.); d.thambiratnam@qut.edu.au (D.P.T.)
[2] School of Engineering, Civil, Environment and Mining Engineering, Faculty of Engineering, The University of Western Australia, Crawley 6009, Australia; mohamed.elchalakani@uwa.edu.au
* Correspondence: sabrina.fawzia@qut.edu.au

Abstract: Rubberised concrete has emerged as a material of interest to the research community with the mission of creating sustainable structural members and decreasing the burden of waste tyre rubber. The potential benefits of replacing natural aggregates with rubber particles to obtain greater energy absorption and ductility are proven in the literature. To negate the reduction in capacity due to the addition of rubber particles, single- and double-skin confinements were proposed and successfully tested by researchers. Hybrid rubberised double-skin tubular columns (RuDSTCs) were recently trialled and tested by the authors. Each of these hybrid RuDSTCs had a filament-wound carbon fibre-reinforced polymer (CFRP) outer tube and an inner steel tube with rubberised concrete as the sandwich material between the two tubes. To explore the axial behaviour of such a column, this paper develops a finite element modelling strategy and carries out a comprehensive parametric study of the hybrid RuDSTC with 0%, 15%, and 30% combined aggregates replaced with rubber particles. This methodology is validated by experimental results, and a good agreement is found. Hybrid RuDSTC models are developed in four groups with different material and geometric parameters, in addition to those corresponding to the experimentally tested column, to explore the effects of the thickness ratio, hollow ratio, steel tube yield strength, and CFRP tube diameter with a special focus on the transition of the characteristic bilinear stress–strain curve of the hybrid RuDSTCs. The results show the smooth transition of the stress–strain curve with increasing rubber content after the yielding of steel, which indicates better ductility of the rubberised columns. The novel hybrid RuDSTCs can provide a promising sustainable solution with greater capacity compared with their unconfined counterparts. Better strain and enhanced ductility of the hybrid RuDSTCs compared with non-rubberized hybrid DSTCs enable their use in seismic-prone regions and mining infrastructure.

Keywords: hybrid RuDSTC; rubberised concrete; filament-wound CFRP; finite element analysis; axial load

Citation: Khusru, S.; Thambiratnam, D.P.; Elchalakani, M.; Fawzia, S. Load–Displacement Behaviour and a Parametric Study of Hybrid Rubberised Concrete Double-Skin Tubular Columns. *Buildings* **2023**, *13*, 3131. https://doi.org/10.3390/buildings13123131

Academic Editor: Daxu Zhang

Received: 17 November 2023
Revised: 12 December 2023
Accepted: 15 December 2023
Published: 18 December 2023

1. Introduction

Every year, a massive quantity of waste tyres is disposed of in landfills all over the world, which creates great concern for the environment. Rubberised concrete (RuC) is produced by replacing a percentage of aggregates in conventional concrete with rubber particles with the objectives of creating a green material and utilising vehicle tyre rubber in a sustainable manner. Previous studies showed that rubberised concrete has several benefits over conventional concrete such as enhanced ductility, greater energy absorption, impact resistance, and improved axial strain capacity [1–4]. However, contrary to these advantages, RuC is also associated with a reduced modulus of elasticity and compressive strength. To minimize this reduction of strength, confinement of the rubberised concrete was proposed with different types of steel- and fibre-reinforced polymers (FRPs). FRPs possess a high strength-to-weight ratio and tailorable mechanical properties, and the successful application

of strengthening steel [5–8] and concrete [9–11] have provided promising backgrounds with ample opportunities for developing innovative high-performance structural members. The confinement effectivity was successfully examined in previous studies, which resulted in the composite column, namely, RuCFST (rubberised concrete-filled steel tube) [12–14], RuCFFT (rubberised concrete-filled FRP tube) [15], RuCFDST (rubberised concrete-filled double-skin tube) [16,17], double-skin tube column (DSTC) with rubcrete [18], and most recently, hybrid RuDSTC (hybrid rubberised double-skin tubular column) as proposed by the authors of this paper based on an experimental investigation [19]. A hybrid RuDSTC is composed of a filament-wound CFRP exterior tube, steel interior tube, and rubberised concrete as the infill material between the tubes. The combination of the three materials as an integrated column offers greater flexibility, deformability, and capacity compared to the traditional columns. The proposed innovative columns have the potential for use as structural columns, especially those vulnerable to vehicular impacts such as bridge piers or columns in car parks.

From the existing literature, it can be recognized that there have been some experimental investigations on the behaviour of composite columns made with rubberised concrete. However, numerical studies, including parametric studies, conducted using finite element (FE) techniques to supplement the test results are very limited. Duarte et al. [12] carried out a numerical investigation on the strength and ductility of short RuCFST columns based on their previous experimental work. Khusru et al. investigated circular RuCFDST columns under axial compression using the material constitutive model proposed by Mander et al. [20] and compared the results with the existing analytical models [16]. The inclusion of rubber particles in these hybrid columns could potentially enhance their energy absorption capacity, thereby potentially bolstering their seismic or dynamic characteristics. Understanding seismic characteristics and effective numerical simulation will enhance the comprehension of its dynamic nature [21–23]. Furthermore, a square RuCFDST was studied by Ayough et al. [17] with 5%, 15%, and 30% rubberised concrete to investigate the effects of material and geometric parameters. The authors of this paper recently published a paper [19] on hybrid columns including limited experimental results. There is no research available on the effects of different parameters of the mentioned hybrid rubberised columns. Therefore, the primary objective of this research is to investigate the axial behaviour and characteristics of RuDSTCs using finite element modelling and a comprehensive parametric study, varying rubber content and geometric parameters. The hypothesis posits that increasing rubber content in these columns will lead to a smoother transition in the stress–strain curves after steel yielding, indicating improved ductility and enhanced capacity compared with their non-rubberized counterparts.

2. Experimental Investigation

The behaviour of hybrid RuDSTCs with filament-wound CFRP exterior tubes was explored experimentally by the authors of this paper [19]. Six stub columns were prepared with 0%, 15%, and 30% rubberised concrete as the infill material between the outer filament-wound tube and the inner steel tube. The compressive strength of the control concrete was 50.13 MPa. The maximum size of the coarse aggregates used was 10 mm, and the other aggregates included 7–10 mm and 1–4 mm crushed rock. Two different sizes of rubber (1–5 mm and 7–10 mm) were obtained from scrap tyres and used to replace the fine and coarse aggregates, respectively. The grain size of the fine sand was 0.2–6 mm, and Portland cement was used as the binding material. The experimental strength of the 15% and 30% rubberised concrete was 24.86 MPa and 9.75 MPa, respectively. A filament-wound CFRP tube with a 152 mm diameter and a 2.5 mm thickness made up of 20%, 20%, and 40% fibres oriented at $\pm 15^{\circ}$, $\pm 40^{\circ}$, and $\pm 75^{\circ}$, respectively, was used as the outer layer. The CFRP tube was tested under compression, and the longitudinal strength and strain in the axial direction were 135 MPa and 0.0084, respectively. The modulus of elasticity in the hoop direction was considered as 66.7 GPa and hoop strength as 592.8 MPa, according to the test results of Li et al. [24] on similar tubes. A C250LO-grade circular hollow tube with a

60.3 mm diameter and a 3.6 mm thickness was used as the inner tube of the composite columns. The height of all the stub columns was 300 mm. The label of the specimen consists of "C" for CFRP followed by the inner steel tube diameter, percentage of rubber replacement (0%, 15%, or 30%), and "I" or "II" for the identical specimens. For example, C-I60-30-I refers to the double-skin specimen with a CFRP outer tube and an I60 inner steel tube with a 60 mm diameter with a rubber replacement ratio of 30%, where I indicates that it is the first of the two identical specimens.

The specimens were concentrically placed on the lower compression platen and a 60 mm thick steel plate was placed at the top of the specimen at the time of testing, as shown in Figure 1a. The axial compression loading was uniformly applied to the specimens using a 500-tonne load cell at a displacement rate of less than one mm per minute.

(**a**)

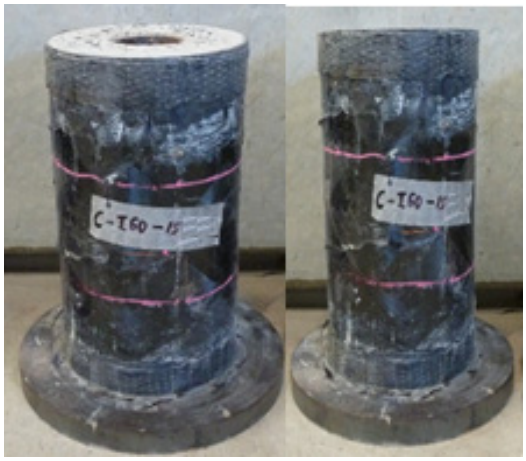

(**b**)

Figure 1. (**a**) Test set up. (**b**) Deformed specimens after testing.

The readings of the compressive loads and corresponding displacements were recorded until a loud bang sound occurred, which indicated the final rupture of the CFRP tube. The initiation of the first crack was associated with a sharp snapping sound due to the damage to the resin of the filament-wound CFRP tube. Even after the first crack, the concrete enclosed with the CFRP tube continued to show an increase in axial capacity. The occurrence of the first cracks was delayed for the rubberised hybrid RuDSTC specimens compared with the control specimens. The slight drops in the load–displacement curve indicate the cracks developed in the filament-wound tube. As the loading progressed, the cracks in the CFRP tube increased due to the lateral pressure exerted by the enclosed concrete, which appeared

mostly in the top and bottom one-third region for all rubberised and non-rubberised stub columns, as can be seen in Figure 1b. The details of the experimental analysis and results are available in Khusru et al. [19].

3. Finite Element Modelling

The experimental study outlined in Khusru et al. [19] involved limited parameters. To understand the complete behaviour of hybrid RuDSTCs, a detailed parametric study was conducted in this paper.

Firstly, the FE modelling strategy was developed using the three-dimensional finite element (FE) software ABAQUS CAE [25] to perform the static monotonic numerical simulation considering nonlinear geometrical analysis using the modified RIKS method. The results obtained from the experimental study by the authors were used to validate the developed numerical model and to conduct simulations by comparing the results. Modelling concrete between two different material tubes is difficult. Moreover, the addition of rubber into concrete as the filler material makes it more complex due to the scarce availability of information on modelling rubberised concrete. The following section presents the development of the numerical model of the filament-wound CFRP-enclosed short hybrid RuDSTCs based on the experimental investigation. The description of the FE model is outlined in Figure 2.

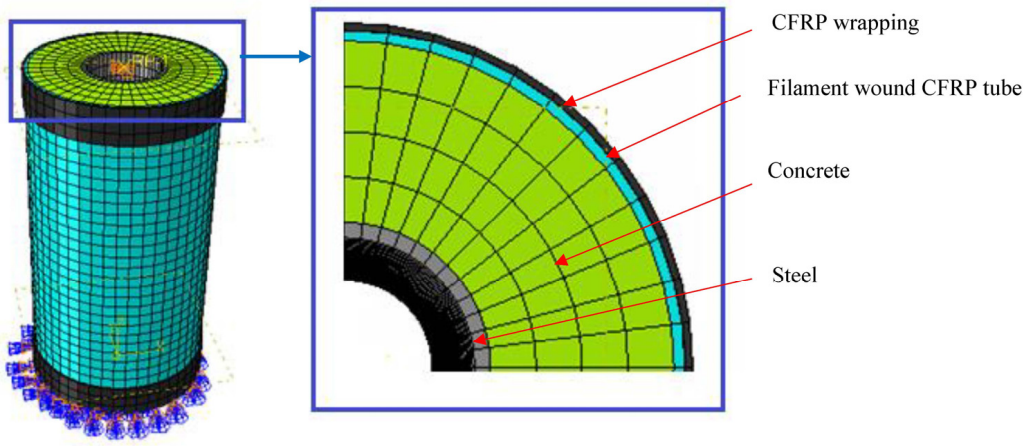

Figure 2. Overview of the 3D model and its components.

3.1. Element Type and Meshing

The first and most important step of finite element analysis is to develop the geometric model of the intended specimen. The accuracy of the results depends on the correct selection of element types. The modelling of an RuDSTC is critical as it involves three different materials. A circular hollow steel tube was modelled using four-node shell elements S4R with hourglass control and reduced integration. The element type chosen for normal and rubberised concrete was C3D8R, depicting an eight-node solid element with reduced integration and hourglass control. The filament-wound CFRP tube was modelled using linear quadrilateral conventional shell elements S4R. Based on the mesh convergence study, the optimum element size that would give the lowest computational time was selected. The mesh element size of $\frac{D}{15}$ was used, similar to Tao et al. [26] for circular tubes. Meshing was performed using the seed elements command in ABAQUS software to keep the number of elements of all three different parts of the model the same by adjusting the element size below $\frac{D}{15}$. The element shape was quad-dominated an advancing front.

3.2. Material Model

The material models considered in the development of the hybrid RuDSTCs are discussed below.

3.2.1. Filament-Wound CFRP Tube

The orthotropic material model was used in the simulation of the CFRP tubes. The composite layup option of ABAQUS was used to provide the layup orientation and properties efficiently. Thickness was assigned from the bottom surface of the cylindrical tube to have proper bonding between the concrete and filament-wound tube. For simulating the damage behaviour, Hashin damage criteria [27] were used, similar to Toh et al. [28]. The elastic properties and transverse and longitudinal strength properties were provided from the experimental observation of the authors and also from the results obtained by Li et al. [24] using similar tubes.

3.2.2. Rubberised Concrete

Several concrete material models are available in the material library of ABAQUS. Among these models, the concrete damage plasticity model (CDPM) was chosen as it showed reasonably accurate predictions for various concrete types [10] under uniform and non-uniform confinement of the FRP jacket [9,29] and also for steel-confined concrete [12]. CDPM was first introduced by Lubinar for assessing performance under monotonic loading [30]. This model requires separate inputs of concrete elastic parameters, plasticity parameters such as the shape factor $K_{c,}$ the ratio of biaxial to uniaxial compression stress $\frac{f_{bO}}{f'_c}$, dilation angle, eccentricity, viscosity, tension, and compression subroutine with the damage parameter. To allow different yields and triaxial tension and compression stresses, the yield surface of CDPM is noncircular in shape and governed by the ratio of second stresses variant of tension and compression at the same hydrostatic stress denoted by K_c [31], which can be obtained from the following equation [32].

$$K_c = \frac{5.5\, f_{bo}}{3f'_c + 5f_{bo}} \tag{1}$$

In the above equation, the K_c value is related to the ratio $\frac{f_{bo}}{f'_c}$, which can be obtained from the following empirical equation by Papanikolaou and Kappos [33].

$$\frac{f_{bO}}{f'_c} = 1.5\,(f'c)^{-0.075} \tag{2}$$

where f'_c is in MPa.

Using both equations of plasticity parameters, the dilation angle for confined normal and rubberised concrete was considered as 20° initially and later modified by conducting sensitivity analysis.

Similar to the studies by Khusru et al. [16] and Ayough et al. [17], the rubberised concrete model suggested by Bompa et al. [34] was used in this study. The stress–strain model of rubberised concrete was developed in three stages using inputs of unconfined compressive strength f_{co}, the rubber replacement ratio ρvr, aggregate size replaced with rubber particles γ, and the elastic modulus in the equations. The first stage denotes the elastic stage, which showed a linear behaviour up to 30% of the unconfined compressive strength of concrete. The corresponding strain $\varepsilon_{rc,el}$ can be calculated using the modulus of elasticity E_{rc} of the concrete. The next stage reflects the elastic–plastic behaviour of concrete for strains ε within the limit of $\varepsilon < \varepsilon_{rc,el} < \varepsilon_{rc,1}$, where $\varepsilon_{rc,1}$ indicates the crushing strain of concrete. The final stage is the post-peak stage for strains $\varepsilon > \varepsilon_{rc}$, which is a function of the post-peak energy and compressive strength f_{rc} of rubberised concrete. Based on the above discussion, the equations of the model can be summarised as below, where ε_{rcu} = ultimate strain of unconfined rubberised concrete and $f_{rc,2}$ = strength of unconfined rubberised concrete.

Stage 1: For $\varepsilon \leq \varepsilon_{rc,el}$

$$\sigma = \varepsilon E_{rc} \tag{3}$$

$$\varepsilon_{rc,el=\frac{0.3\ f_{rc}}{E_{rc}}} \tag{4}$$

$$f_{rc} = \frac{f_{co}}{1 + 2(1.5\gamma\rho\upsilon r)^{3/2}} \tag{5}$$

Stage 2: For $\varepsilon_{rc,el} < \varepsilon < \varepsilon_{rc,l}$

$$\sigma = \left[\frac{5}{3}\left(\frac{\varepsilon - \varepsilon_{rc,el}}{\varepsilon_{rc1}}\right) - \left(\frac{\varepsilon - \varepsilon_{rc,el}}{\varepsilon_{rc1}}\right)^2 + 0.3\right] f_{rc} \tag{6}$$

Stage 3: For $\varepsilon \geq \varepsilon_{rcu}$

$$\sigma = \left[\frac{1}{8}\left(\frac{{f_{rc}}^{\frac{1}{3}}}{(1+\rho\vartheta r)^{\frac{2}{3}}} - 1\right)^2 \left(\frac{\varepsilon - \varepsilon_{rc1}}{\varepsilon_{rc1}}\right)^2 - \frac{6}{8}\left(\frac{{f_{rc}}^{\frac{1}{3}}}{(1+\rho\vartheta r)^{\frac{2}{3}}} - 1\right)\left(\frac{\varepsilon - \varepsilon_{rc1}}{\varepsilon_{rc1}}\right) + \frac{f_{rc,2}}{f_{rc}}\right] f_{rc} \tag{7}$$

$$\frac{f_{rc,2}}{f_{rc}} = \frac{5}{3}\left(\frac{\varepsilon - \varepsilon_{rc,el}}{\varepsilon_{rc1}}\right) - \left(\frac{\varepsilon - \varepsilon_{rc,el}}{\varepsilon_{rc1}}\right)^2 + 0.3 \tag{8}$$

3.2.3. Steel

The bilinear stress–strain model of steel suggested by Han et al. [35] was used as the material model of the inner tube in the numerical analyses by Pagoulatou et al. [36] and Khusru et al. [16]. This model consists of a linear elastic phase followed by a perfectly plastic phase. In ABAQUS, steel is elastic up to the yield strength, and it is considered plastic from the yield point to the final strain value of 3%. This model was used for the present numerical simulations. The modulus of elasticity was considered as 200,000 MPa and Poisson's ratio as 0.3.

3.2.4. CFRP Wrapped at the Top and Bottom

To prevent premature failure, three layers of CFRP sheets were wrapped at the top and bottom of the specimen in the experimental investigation. As the stiffness of the CFRP sheet is negligible in the loading direction, interlayer delamination was not observed. To avoid complexity, the CFRP was modelled as linear elastic brittle material in the ABAQUS material model and as a continuum shell element with no compression option by setting Poisson's ratio to zero, similar to the study by Zeng et al. [9]. The thickness of the CFRP layer was taken as 0.6 mm, and the same properties of the CFRP sheet were used in the experimental investigation performed by Khusru et al. [19] was used in this analysis.

3.3. Surface Interaction and Boundary Conditions

Surface-to-surface interaction was used to create bonding between the steel–concrete, concrete-CFRP tube, and CFRP tube-CFRP wrap surface. The master–slave contact algorithm was used in these surface pairs, in which the master surface was allowed to penetrate the slave surface. The tie constraint was used between the surfaces and connected the nodes of the surfaces. To prevent the penetration of the surfaces under compression, 'Hard contact' was chosen as the contact overclosure, and a friction coefficient of 0.3 was used in the Coulomb friction model.

The hybrid column is considered as the pin-ended column loaded at the top. The compressive load applied at the top of the column suppressed the hybrid column, activating the confinement of the FRP and causing similar deflection in all three component materials of the column. To replicate this behaviour, boundary conditions were applied at the top and the bottom of the specimen numerical model. The top nodes of the model were constrained using an independent reference point located at the centre of the top surface using multiple point constraints (MPCs). Loading was applied through this reference point and to match the experimental loading applied at the top; the reference point was restricted to downward

vertical movement only but allowed all rotational degrees of freedom. The bottom nodes of the specimen were restricted from all translational and rotational degrees of freedom with the boundary condition ENCASTRE listed in the model tree. The validation of stub hybrid RuDSTCs involves a two-step process of analysis. Firstly, a buckling analysis was conducted using the linear perturbation step in ABAQUS software to predict the buckling mode involving three buckle shapes of the column. The nodal displacement for the buckling mode was used in the second step of FE analysis using the Static RIKS method.

4. Validation of the Numerical Model

The results obtained from the numerical simulation were compared with the experimental results to validate the FE simulation technique. Figure 3 represents the axial load–axial displacement curves of the 0%, 15%, and 30% RuDSTCs obtained from the experimental investigation by the authors [19] and the FE simulations carried out in this paper. It is evident that the two sets of results agree well with very small variations.

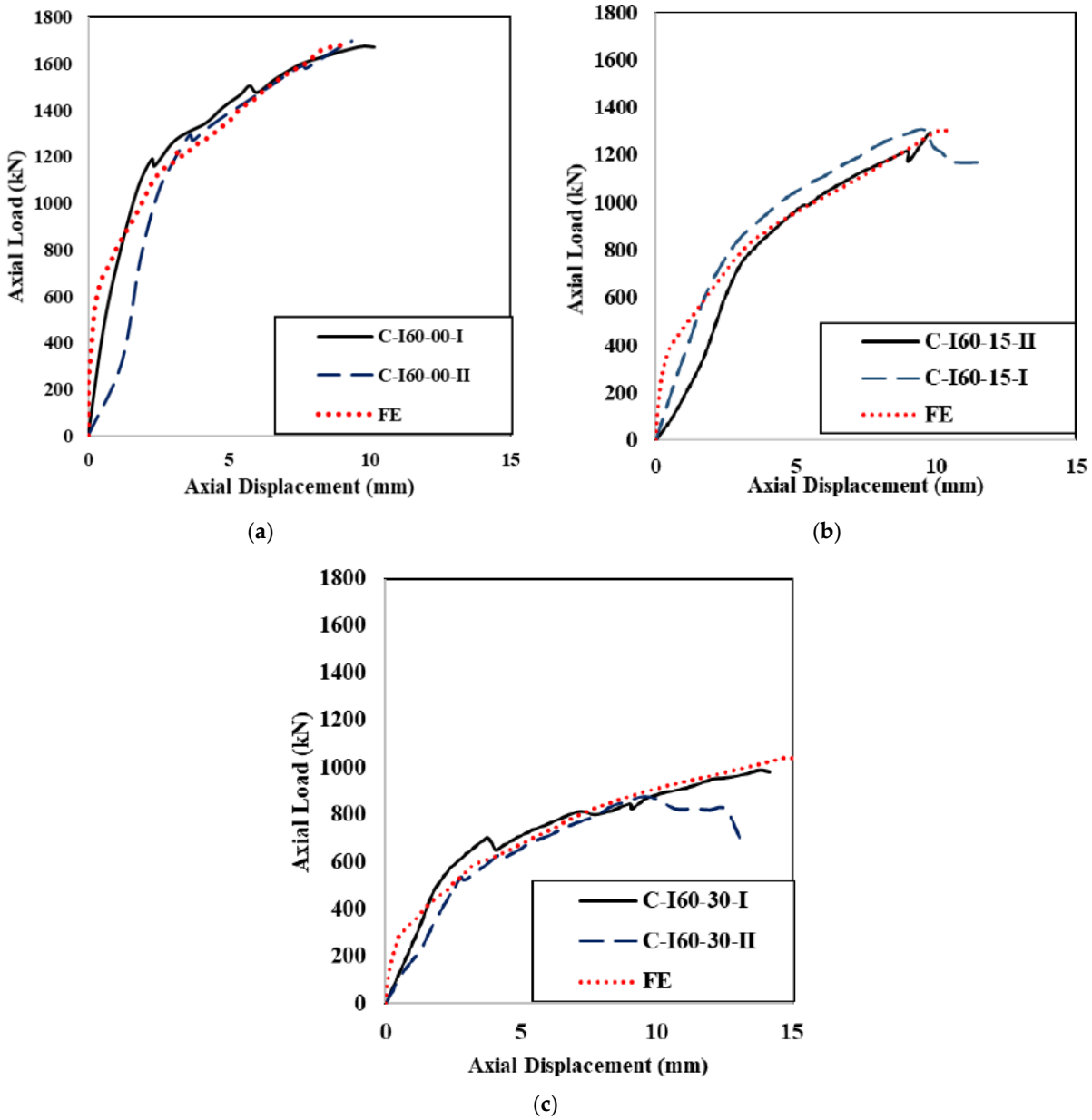

Figure 3. Comparison of axial load–axial displacement curves obtained from experiments and FE simulations of 0%, 15%, and 30% RuDSTCs: (**a**) 0% RuDSTCs, (**b**) 15% RuDSTCs, and (**c**) 30% RuDSTCs.

Similar to the experimental observation, the FE simulation showed that the increase in rubber content decreases the overall capacity of the column but results in a flatter second part of the load–displacement curve, indicating more ductile behaviour. Table 1 shows the axial load capacities obtained from the validated numerical model along with the experimental results. The results match closely with a mean ratio of 0.941 and COV is 0.043. Good agreement between the experimental and FE results validates the modelling technique used in this paper.

Table 1. Comparison of the experimental and FE results.

Specimen	P_{FE}	P_{EXP}	P_{EXP}/P_{FE}
	kN	kN	
C-I60-00-I	1792	1671	0.93
C-I60-00-II	1792	1692	0.94
C-I60-15-I	1329	1314	0.98
C-I60-15-II	1329	1286	0.97
C-I60-30-I	1034	987	0.95
C-I60-30-II	1034	888	0.86

The load–displacement curves of the hybrid RuDSTCs, obtained from the experimental observations by the authors [19] and also from the hybrid columns investigated by Lam et al. [37], Zhang et al. [11], and Li et al. [24] with varying infill material, showed a typical bilinear pattern. Figure 4 shows the main features of the axial load vs. axial displacement curve of the hybrid RuDSTC.

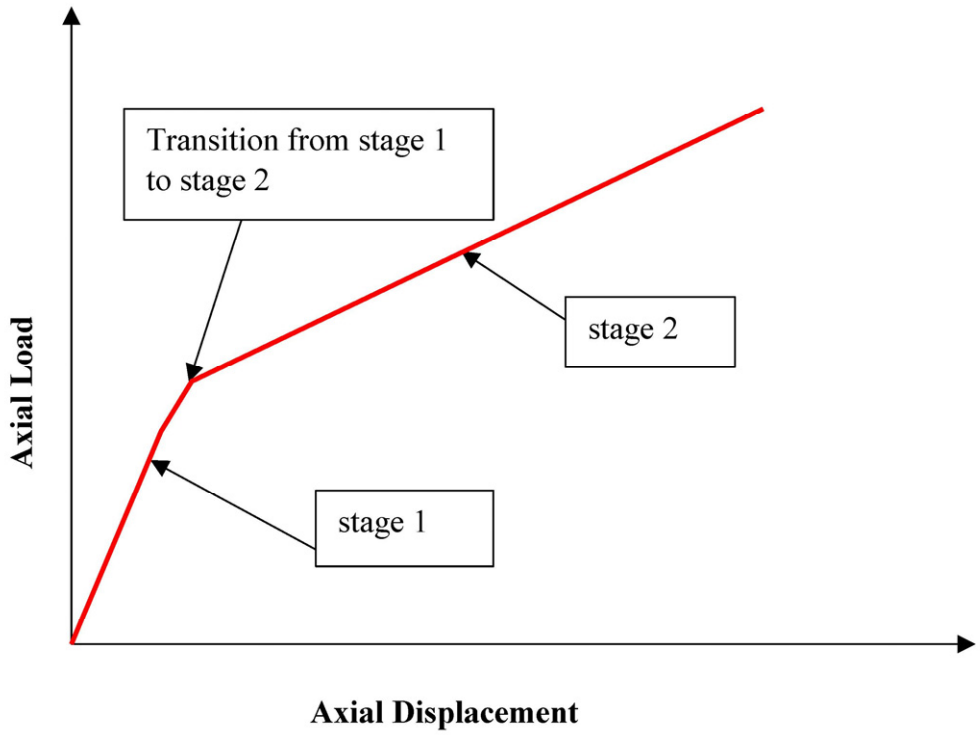

Figure 4. Typical axial load–axial displacement curve of the hybrid RuDSTC.

The graph in Figure 4 represents three important features, namely, Stage 1: the parabolic first part and Stage 2: a linear second part and a smooth transition with the yielding of the inner steel tube, which marks the beginning of the stage 2.

5. Parametric Study

All the rubberised and non-rubberised hybrid specimens investigated by Khusru et.al. [24] showed a bilinear load–displacement relationship, as shown in Figure 5, which was also reported by previous researchers of hybrid columns with different infill materials [11,18,24,38]. The first stage of the curve started with the initiation of loading and continued until the occurrence of the yielding of the steel tube. During this stage, the CFRP tube was activated and expanded in the lateral direction. The second stage started with tube yielding and continued until the failure of the specimen. To understand the effects of different parameters on the transition from Stage 1 to the final stage, this paper developed and analysed stub hybrid RuDSTC column models in four groups. Table 2 presents the details of the specimens considered in the parametric study, in which one parameter of a group of specimens was varied at a time while keeping all other parameters constant. The length of all the columns was 300 mm, and each configuration of the column was analysed for 0%, 15%, and 30% rubberised concrete, keeping the concrete strength the same as the experiment.

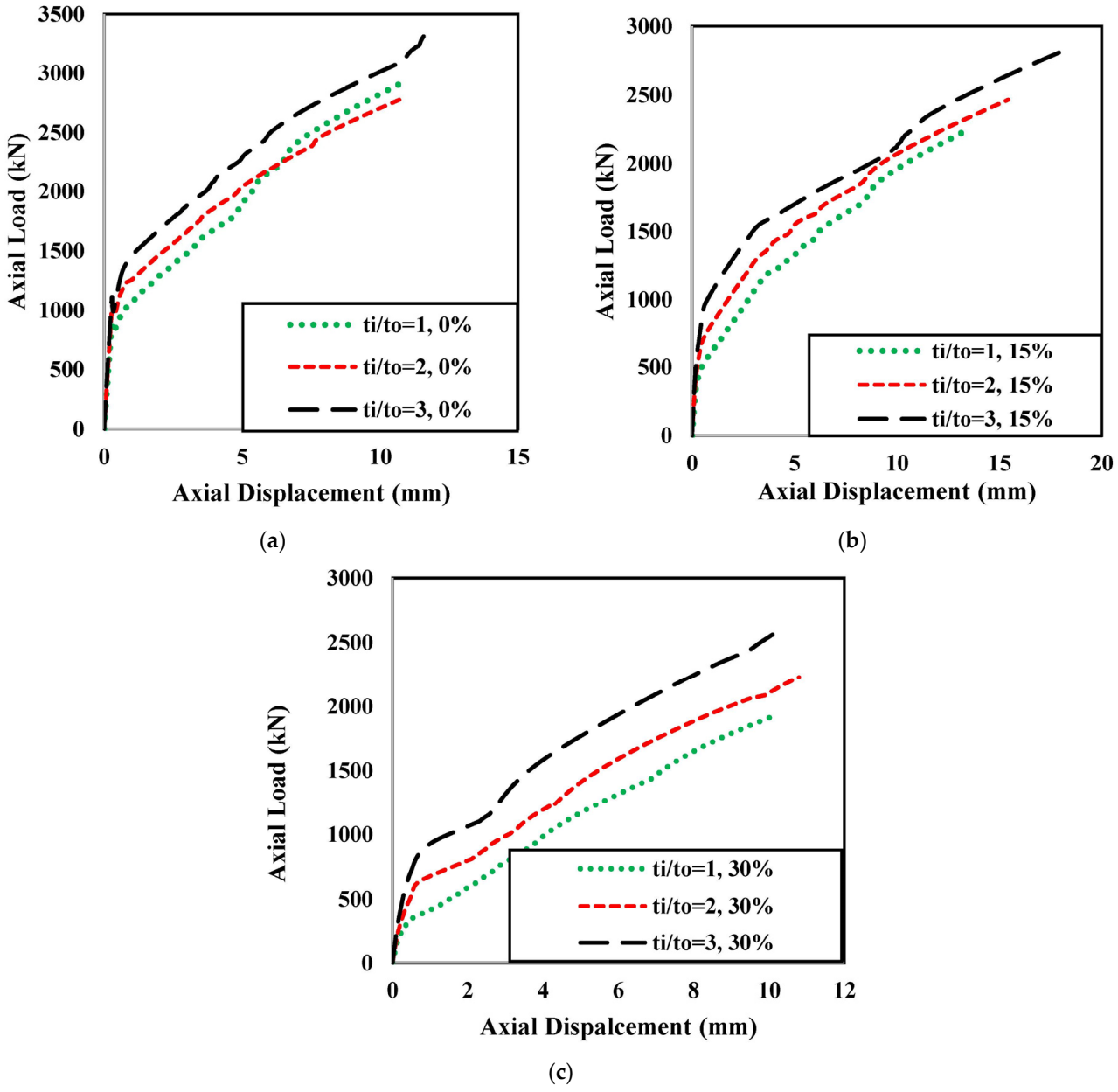

Figure 5. Effect of the thickness ratio: (**a**) 0% RuDSTCs, (**b**) 15% RuDSTCs, and (**c**) 30% RuDSTCs.

Table 2. Details of the specimens in the parametric study.

Specimen ID	% Rubber	FRP Tube		Steel Tube			Control Concrete Strength
		D_o (mm)	t_o (mm)	D_i (mm)	t_i (mm)	f_y (mm)	f'_c (MPa)
Group 1, thickness ratio							
t_i/t_o = 1, 0%	0%	200	2.5	101.6	2.5	250	50
t_i/t_o = 1, 15%	15%	200	2.5	101.6	2.5	250	
t_i/t_o = 1, 30%	30%	200	2.5	101.6	2.5	250	
t_i/t_o = 2, 0%	0%	200	2.5	101.6	5.0	250	50
t_i/t_o = 2, 15%	15%	200	2.5	101.6	5.0	250	
t_i/t_o = 2, 30%	30%	200	2.5	101.6	5.0	250	
t_i/t_o = 3, 0%	0%	200	2.5	101.6	7.5	250	50
t_i/t_o = 3, 15%	15%	200	2.5	101.6	7.5	250	
t_i/t_o = 3, 30%	30%	200	2.5	101.6	7.5	250	
Group 2, hollow ratio							
HR = 0.30, 0%	0%	200	2.5	60.3	5.0	250	50
HR = 0.30, 15%	15%	200	2.5	60.3	5.0	250	
HR = 0.30, 30%	30%	200	2.5	60.3	5.0	250	
HR = 0.50, 0%	0%	200	2.5	101.6	5.0	250	50
HR = 0.50, 15%	15%	200	2.5	101.6	5.0	250	
HR = 0.50, 30%	30%	200	2.5	101.6	5.0	250	
HR = 0.80, 0%	0%	200	2.5	159	5.0	250	50
HR = 0.80, 15%	15%	200	2.5	159	5.0	250	
HR = 0.80, 30%	30%	200	2.5	159	5.0	250	
Group 3, steel tube yield strength							
f_y = 250, 0%	0%	152	2.5	60.3	3.6	250	50
f_y = 250, 15%	15%	152	2.5	60.3	3.6	250	
f_y = 250, 30%	30%	152	2.5	60.3	3.6	250	
f_y = 350, 0%	0%	152	2.5	60.3	3.6	350	50
f_y = 350, 15%	15%	152	2.5	60.3	3.6	350	
f_y = 350, 30%	30%	152	2.5	60.3	3.6	350	
f_y = 450, 0%	0%	152	2.5	60.3	3.6	450	50
f_y = 450, 15%	15%	152	2.5	60.3	3.6	450	
f_y = 450, 30%	30%	152	2.5	60.3	3.6	450	
Group 4, diameter of CFRP tube							
O114, 0%	0%	114	3.0	60.3	3.6	250	50
O114, 15%	15%	114	3.0	60.3	3.6	250	
O114, 30%	30%	114	3.0	60.3	3.6	250	
O165, 0%	0%	165	3.0	60.3	3.6	250	50
O165, 15%	15%	165	3.0	60.3	3.6	250	
O165, 30%	30%	165	3.0	60.3	3.6	250	

The first group of specimens analyses the effect of the thickness ratio (ratio of the thickness of steel tube to that of CFRP tube) to understand the confinement effect provided by the double tubes. The first specimen in this group is designated by t_i/t_o = 1, 0%, where the first value indicates that the thickness ratio is 1 and the second value indicates the percentage of rubber. The second group comprises specimens with varying hollow ratios (ratio of the inner steel tube diameter to the outer CFRP tube diameter). The specimens in this group are designated by the value of the hollow ratio "HR" followed by the percentage of rubber. For the hybrid column, larger void ratios of 0.7 to 0.8 are desirable for the sustainable use of the void for running pipelines or electrical wirings [11]; however, considering this value, the authors studied the range of 0.3 to 0.8 to obtain an overall picture of the effect of the hollow ratio. The third group examines the effect of steel tube yield strength, as several steel grades are available for construction. The first specimen in this group is designated as f_y = 250, 0%, where the first value indicates the yield strength of the steel tube and the second value indicates the percentage of rubber. The fourth group highlights

the effect of variation in the CFRP tube diameter keeping the same thickness and is named O165, 0%, where O165 indicates that the outer CFRP tube of the hybrid column has a diameter of 165 mm and the column is filled with 0% rubberised concrete. Considering the thickness of the CFRP tube as 3 mm, the experimental values of the modulus of elasticity and failure strength of the selected tubes were considered from the study by Li et al. [24].

The selection of these specific parameters was driven by their direct influence on the structural behaviour and performance of rubberized concrete-filled double-skin tubes with an FRP tube outer and steel inner. The thickness ratio and hollow ratio directly impact load-bearing capacity, material optimization, and construction feasibility, aligning with real-world design considerations for balanced strength and economical use of materials. Additionally, investigating the effects of steel tube yield strength and CFRP tube diameter addresses crucial practical concerns related to structural integrity, safety margins, and the potential for weight reduction, reflecting their pivotal roles in informing efficient and reliable designs for practical applications in construction and infrastructure.

5.1. Effect of the Thickness Ratio

The thickness ratio of the hybrid column t_i/t_o is defined as the ratio of the inner tube thickness t_i to the outer tube thickness t_o. For the parametric study, the outer CFRP tube thickness was kept constant at 2.5 mm, similar to the tube tested by Khusru et al. [19], and the inner steel tube thickness was varied considering 2.5 mm, 5 mm, and 7.5 mm, which gives the range of thickness ratio from 1 to 3 with all other parameters of the column remaining unchanged. The results of the parametric study are presented in Figure 5. Figure 5 depicts that the axial capacity of hybrid RuDSTCs is enhanced with the increase in the steel tube thickness. However, for the same thickness ratio, the axial capacity of the column decreases with the increase in rubber content.

For the 30% rubberised columns, a more uniform loss of strength can be observed with increasing rubber content. The transition between Stage 1 and Stage 2 is prolonged. The axial capacity at transition for the similar outer and inner tube is 1379 kN, which is decreased by 34.09% and 42.64% for the 15% and 30% rubberised concrete, respectively. However, the axial displacement at transition increased to 32.80% and 106.20% for the 15% and 30% hybrid RuDSTC columns, respectively. For thickness ratio t_i/t_o = 2, the transition between the stages appeared at 1239 kN, which reduced to 40.5% and 51.5% when incorporating 15% and 30% rubber, respectively.

5.2. Effect of the Hollow Ratio

The hollow ratio of a hybrid RuDSTC represents the ratio of the inner steel tube diameter to the outer CFRP tube diameter. The hollow ratios considered for the parametric study were 0.3, 0.5, and 0.8. The effect of the hollow ratio was observed by keeping the outer CFRP tube diameter constant at 200 mm and changing the interior steel tube diameter to 60.3 mm, 101.6 mm, and 159 mm, respectively.

Figure 6 represents the effect of the hollow ratio on the control and rubberised concrete columns. With an increase in the hollow ratio, the strength of the column decreases, which results in a reduced sandwiched concrete area for both the normal and rubberised concrete. This trend is similar to the experimental observations by Li et al. [24] with seawater–sea sand concrete and Zhang et al. [11] with high-strength concrete. The load before the transition was observed in the columns with a higher hollow ratio, which ceases with increasing rubber content for the same hollow ratio. The stiffer first stage of the bilinear curve was observed for the 0% rubberised concrete compared with the rubberised columns. For the 0% hybrid RuDSTC, the transition to the second stage occurs at 1482 kN for HR = 0.3, 942 kN for HR = 0.5, and 933 kN for HR = 0.8. The second stage of the bilinear curve is less stiff for the 30% rubberised concrete for the same hollow ratio. The transition of the first stage to the second stage of the bilinear curve of the hybrid DSTC tends to be smoother with an increasing hollow ratio, indicating more ductile behaviour of the columns. For the

30% RuDSTC, an extended transition between the first and second stages is observed for varying hollow ratios of 0.3 to 0.8.

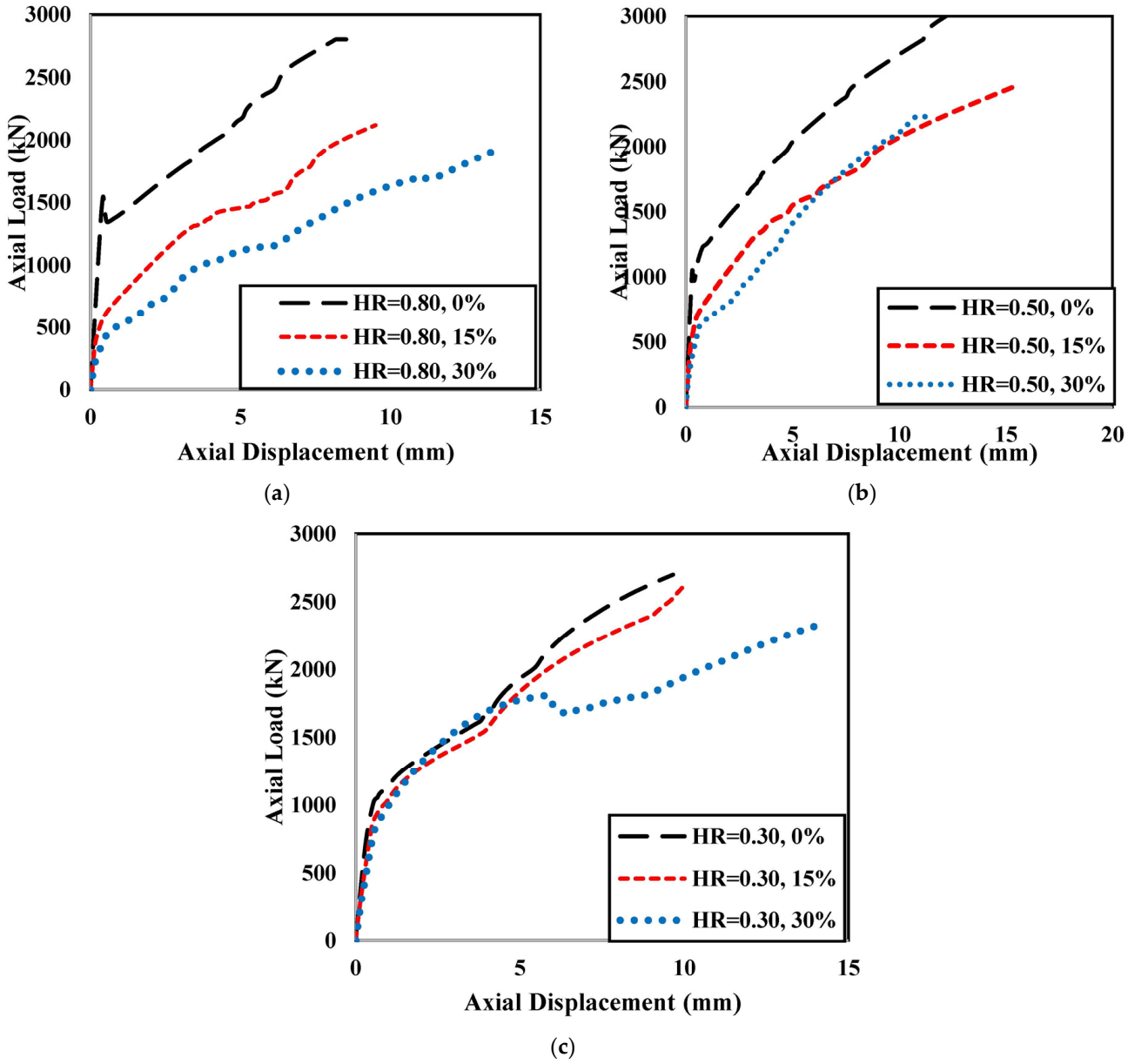

Figure 6. Effect of the hollow ratio: (**a**) 0% RuDSTC, hollow ratio = 0.80, (**b**) 15% RuDSTC, hollow ratio = 0.50, and (**c**) 30% RuDSTC, hollow ratio = 0.30.

5.3. Effect of Steel Tube Yield Strength

The yield strength of a steel tube is an important parameter of a hybrid RuDSTC column as the behaviour of the steel tube is largely dependent on the yield value, and several strength grades are used in construction.

To understand the effect of this parameter, yield strengths of 250 MPa, 350 MPa, and 450 MPa were chosen for the FE analysis of the Group 4 specimens in Table 2 for the 0%, 15%, and 30% rubberised concrete. The results are presented in Figure 7.

As per Figure 7, the axial load capacity of the column is enhanced with an increasing value of yield strength for both the rubberised and non-rubberised columns. However, for the same strength of the inner steel tube, increasing the percentage of rubber resulted in a smoother transition to the second stage from the first stage of the load–displacement curve. A higher grade of steel also showed greater stiffness of the hybrid column. The

yield of the steel tube occurred at the lower load with an increasing percentage of rubber aggregates. For the 30% rubberised concrete, the drop in the axial load was significant in the second stage compared with the 0% and 15% rubberised columns. Transition to the second stage from the first stage started at a similar displacement and load for all three types of concrete for a particular steel grade. The load capacity at transition was enhanced by 39.53% and 153% by increasing the steel tube yield strength from 250 MPa to 350 MPa and 450 MPa, respectively.

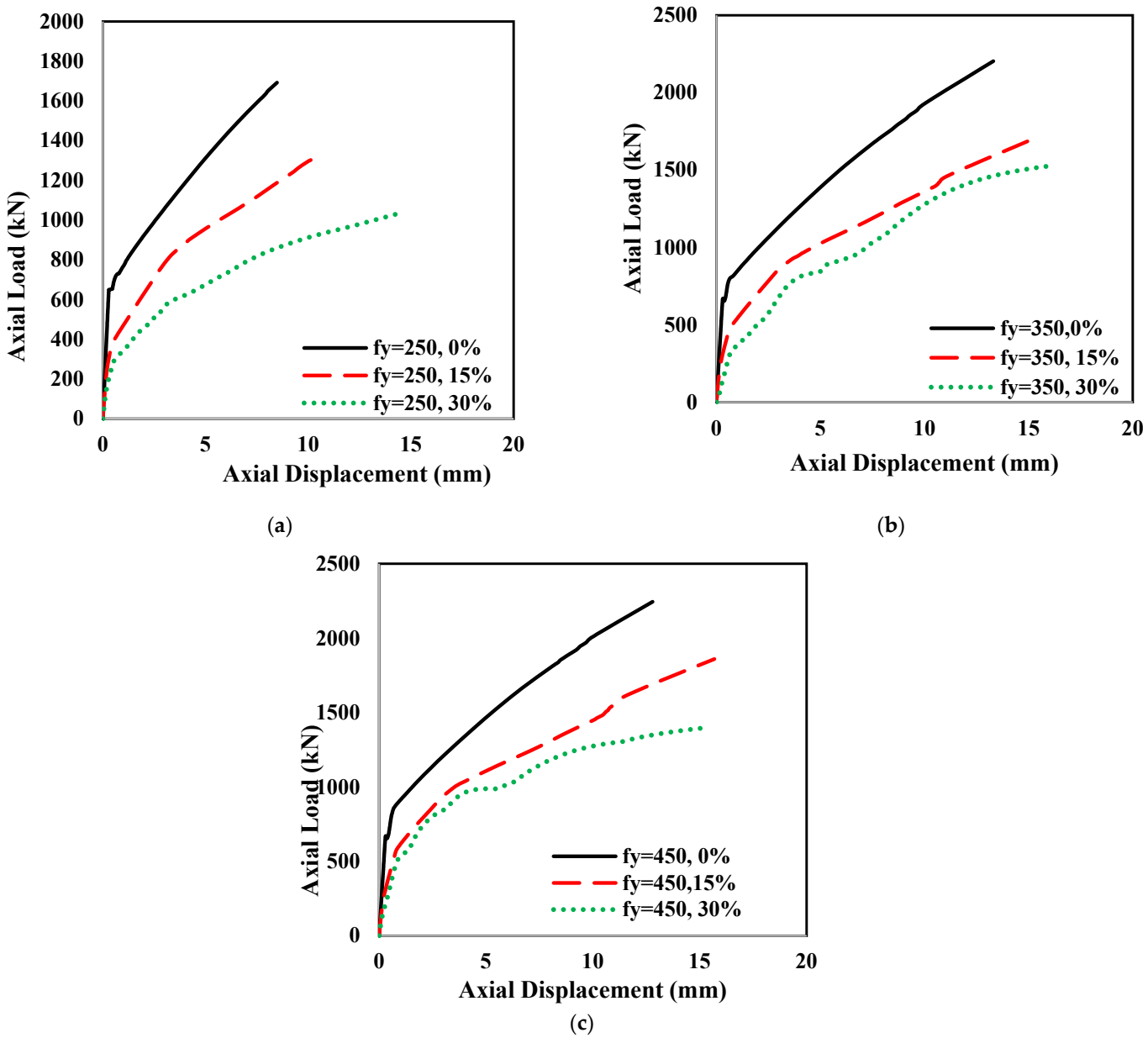

Figure 7. Effect of the steel tube yield strength: (**a**) f_y = 250 MPa, (**b**) f_y = 350 MPa, and (**c**) f_y = 450 MPa.

5.4. Effect of the Diameter of the CFRP Tube

As per the experimental investigation by Li et al. [24], the properties of the CFRP tube for a fixed fibre layup and thickness are not affected by the varying diameter of the tube. The Group 4 specimens shown in Table 2 were developed and analysed to explore the behaviour of the columns with varying outer tube diameters of 114 mm and 165 mm, keeping the inner steel tube diameter, yield strength, and thickness the same for all the columns in this group. The results of the FE analysis are presented in Figure 8.

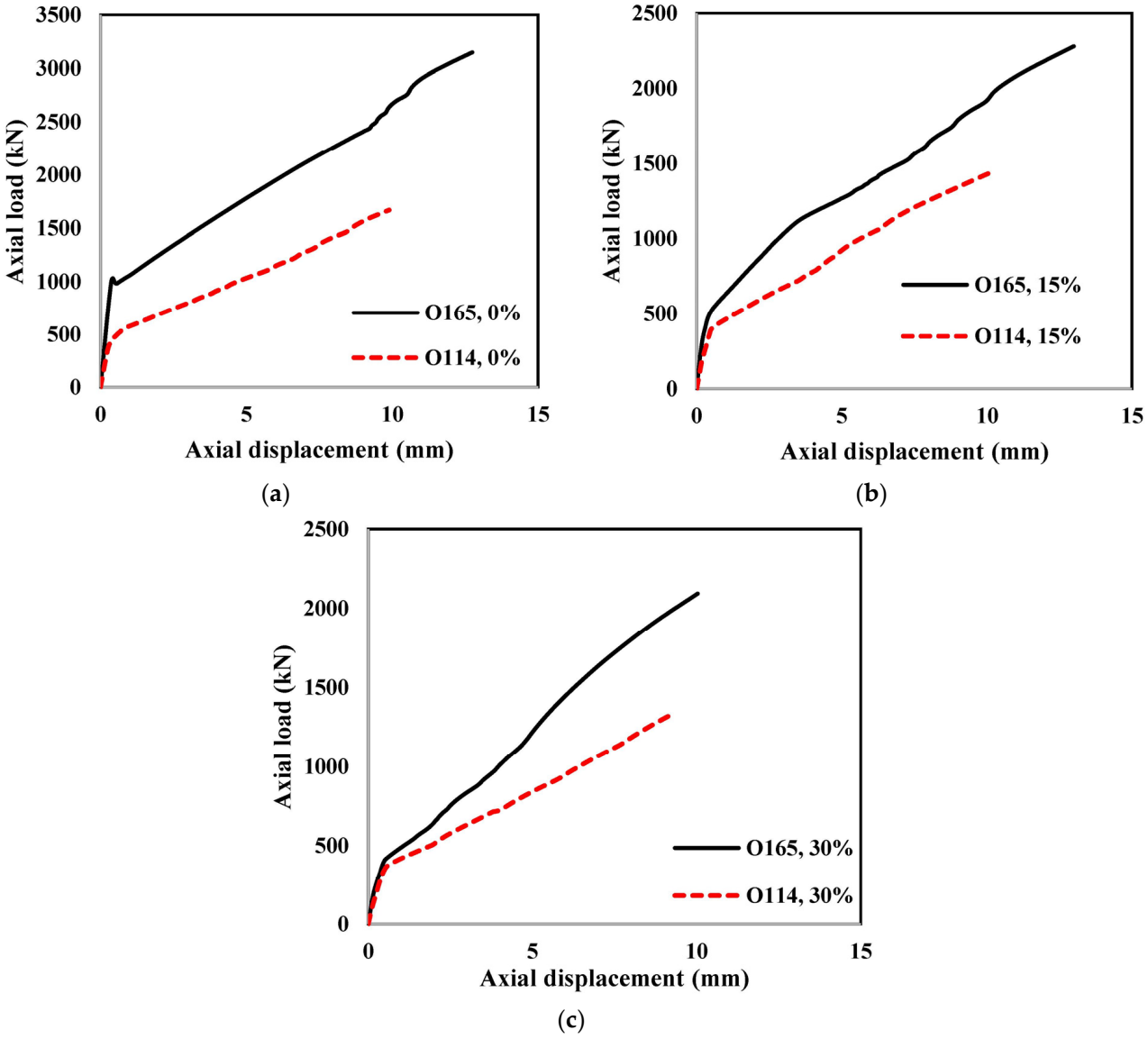

Figure 8. Effect of CFRP tube diameter in (**a**) 0% RuDSTCs, (**b**) 15% RuDSTCs, and (**c**) 30% RuDSTCs.

Figure 8 shows that the axial load capacity of the column increases with the increasing outer CFRP tube diameter as it also increases the area of concrete inside the tubes. However, the larger outer diameter of the CFRP tube resulted in a stiffer second stage of the load–displacement curve of the column. The yielding of the steel tube occurred at a similar displacement for varying CFRP tube diameters, but the axial load value varied significantly for non-rubberised columns. However, with the increasing percentage of rubber, the load difference at transition ceased.

This study enriches existing knowledge by showcasing that a higher rubber content in hybrid RuDSTCs leads to improved ductility post-steel yielding, underscoring potential advancements in seismic and mining infrastructure for more resilient constructions. The broader implications emphasize the promising sustainable solution these columns offer, surpassing the capacities of non-rubberised counterparts and thus expanding possibilities in structural engineering for enhanced resilience in various applications.

6. Comparison with Existing Design Guideline

Teng et al. [39] proposed the simple stress–strain model of FRP-confined circular concrete column, which was based on the earlier model by Lam and Teng [40]. Yu et al. [37]

modified the design-oriented stress–strain model proposed by Teng et al. [39] for a filament-wound double-skin tubular column with concrete infill and an interior steel tube. The equation of confined concrete was given as

$$\frac{f_{cc}{}'}{f_{c0}{}'} = \begin{cases} 1 + 3.5(\rho_k - 0.01)\rho_\varepsilon & \rho_k \geq 0.01 \\ 1 & \rho_k \leq 0.01 \end{cases} \quad (9)$$

where,

$f_{cc}{}'$ = compressive strength of confined concrete;
$f_{c0}{}'$ = compressive strength of unconfined concrete;
ρ_k = confinement stiffness ratio of the FRP tube;
ρ_ε = strain ratio of the FRP tube;
ρs = density of steel.

The confined concrete strength of the hybrid RuDSTCs obtained from the parametric study was compared with the modified model of Yu et al. [37]. The unconfined rubberised concrete strength obtained from the experiment and Equations (3)–(8) were used as the input value of $f_{c0}{}'$ in Equation (9). The remaining parameters of Equation (9) were calculated as per Zhang et.al. [11]. To calculate the confined concrete strength ($f_{cc}{}'$) of the hybrid RuDSTCs, the individual axial capacity of the exterior and interior parts, namely, the filament-wound CFRP tube and the interior steel tube, respectively, was deducted from the overall capacity of the column, and the calculated axial load carried by confined concrete was then converted into the confined stress using the cross-sectional area of the concrete infill.

The value of axial capacity of the interior and exterior tube was taken from the experimental investigation by the authors of this paper [19]. The $f_{cc}{}'$ from FE and those calculated using Yu et al.'s [11] model are presented in Table 3.

Table 3. Comparison of the confined concrete strength of the hybrid columns with the existing design model.

Specimen ID	$f_{cc}{}'_{(FE)}$ MPa	$f_{cc}{}'_{(Yu)}$ MPa	Ratio of $f_{cc}{}'_{(FE)}$ $f_{cc}{}'_{(Yu)}$
t_i/t_o = 1, 0%	107.46	94.78	1.13
t_i/t_o = 1, 15%	78.33	76.01	1.03
t_i/t_o = 1, 30%	65.90	61.97	1.06
t_i/t_o = 2, 0%	93.47	94.78	0.99
t_i/t_o = 2, 15%	76.90	76.01	1.01
t_i/t_o = 2, 30%	60.90	61.97	0.98
t_i/t_o = 3, 0%	118.32	94.78	1.25
t_i/t_o = 3, 15%	92.34	76.01	1.21
t_i/t_o = 3, 30%	79.20	61.97	1.28
HR = 0.30, 0%	78.29	94.78	0.83
HR = 0.30, 15%	75.15	76.01	0.99
HR = 0.30, 30%	65.40	61.97	1.06
HR = 0.50, 0%	107.85	94.78	1.14
HR = 0.50, 15%	79.12	76.01	1.04
HR = 0.50, 30%	69.12	61.97	1.12
HR = 0.80, 0%	136.73	94.78	1.44
HR = 0.80, 15%	77.73	76.01	1.02
HR = 0.80, 30%	61.26	61.97	0.99
f_y = 250, 0%	117.69	111.36	1.06
f_y = 250, 15%	92.38	92.60	1.00
f_y = 250, 30%	47.81	78.56	0.61
f_y = 350, 0%	122.21	111.36	1.10
f_y = 350, 15%	94.88	92.60	1.02
f_y = 350, 30%	89.52	78.56	1.14
f_y = 450, 0%	124.90	111.36	1.12
f_y = 450, 15%	99.72	92.60	1.08
f_y = 450, 30%	69.32	78.56	0.88

Table 3. *Cont.*

Specimen ID	f_{cc}' (FE) MPa	f_{cc}' (Yu) MPa	Ratio of f_{cc}' (FE) f_{cc}' (Yu)
O114, 0%	176.65	134.40	1.31
O114, 15%	145.20	115.64	1.26
O114, 30%	130.66	101.59	1.29
O165, 0%	148.10	105.92	1.40
O165, 15%	101.21	87.15	1.16
O165, 30%	91.12	73.11	1.25
Mean			**1.09**
CV			**0.12**

The predicted value from Yu et al.'s model using the rubberised concrete properties and the FE results of confined rubberised concrete strength correlated reasonably well, as shown in Figure 9, which is indicated by a mean value of 1.05 and a coefficient of variance (CV) 0.17.

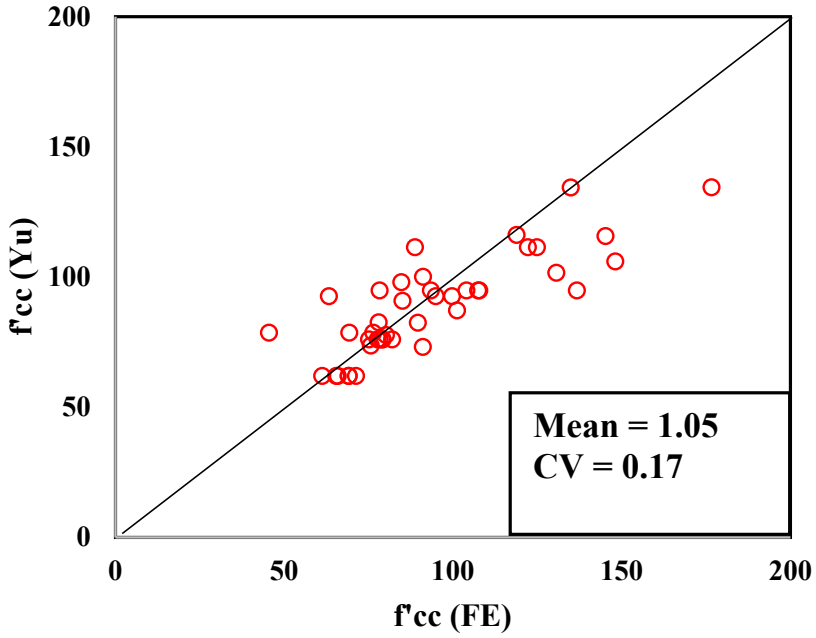

Figure 9. Comparison of confined concrete strength (f_{cc}') from modified Yu et al.'s model [13] against the FE results.

7. Conclusions

In this paper, a detailed parametric study was carried out to understand the behaviour of hybrid RuDSTC columns under axial loading. The numerical model used in this study was validated with the experimental results from the authors' published paper on the experimental investigation of hybrid RuDSTCs with a filament-wound CFRP tube. A detailed parametric study was then carried out to understand the behaviour of hybrid columns in four different groups. The parameters were the thickness ratio, hollow ratio, diameter of the CFRP tube, and yield strength of the steel tube. Bilinear load–displacement curves were observed for all the specimens. However, the behaviour of the columns varied at the transition (which occurs due to the yielding of steel) between the first and second stages of the curve. The parametric study enabled us to capture the effects of four different parameters on the behaviour of the hybrid columns with a special focus on the transition. Based on the results presented in this paper the following conclusion can be drawn.

i. The axial load capacity of the hybrid RuDSTCs is enhanced with an increase in the tube thickness, yield strength of steel, and inner steel tube diameter and a decrease

in the hollow ratio. Increasing the rubber content results in a flatter second stage of the load–displacement curve, indicating ductile behaviour compared with the non-rubberised columns.

ii. For the same thickness ratio, the axial capacity of the column decreases with the increase in the rubber content. Again, for the same strength of the inner tube steel, increasing the percentage of rubber resulted in a smoother transition from the first stage to the second stage of the load–displacement curve. A higher grade of steel also showed a greater stiffness of the hybrid column.

iii. A larger outer diameter of the CFRP tube resulted in a stiffer second stage of the column. The yielding of steel tubes occurred at a similar displacement, but the axial load value varied significantly for the non-rubberised columns.

iv. The strength and stiffness of the hybrid columns decreased with the increasing rubber content. A gradual and smooth transition of the load–displacement curve was observed for the 30% rubberised concrete compared with the 15% non-rubberised concrete.

v. The confined concrete strength of the hybrid RuDSTCs obtained from the parametric study was compared with the results obtained from the modified Yu et al. model using rubberised concrete properties. A good correlation was achieved, which indicated that the modified Yu et al.'s model can be used to predict the capacity of hybrid RuDSTCs.

vi. Further exploration of hybrid columns under varying loading conditions, including long-term cyclic loading, environmental influences, and impact loading, will present an opportunity to deepen our understanding of their structural behaviour and accommodation for practical use.

Author Contributions: Conceptualization, S.K. and S.F.; Methodology, S.K.; Validation, S.K.; Formal analysis, S.K.; Investigation, S.K.; Resources, S.F.; Data curation, S.K.; Writing—original draft, S.K.; Writing—review & editing, D.P.T., M.E. and S.F.; Supervision, D.P.T., M.E. and S.F.; Project administration, S.F.; Funding acquisition, S.F. All authors have read and agreed to the published version of the manuscript.

Funding: This research received no external funding.

Data Availability Statement: The data presented in this study are available on request from the corresponding author. The data are not publicly available due to the data also form part of an ongoing study.

Acknowledgments: The authors would like to thank the Queensland University of Technology (QUT) for providing support (the high-performance computing (HPC) facility, and software for analysis) to carry out the work reported in this paper.

Conflicts of Interest: The authors declare that they have no conflict of interest.

References

1. Bompa, D.; Elghazouli, A.; Xu, B.; Stafford, P.; Ruiz-Teran, A. Experimental assessment and constitutive modelling of rubberised concrete materials. *Constr. Build. Mater.* **2017**, *137*, 246–260. [CrossRef]
2. Najim, K.; Hall, M. A review of the fresh/hardened properties and applications for plain-(PRC) and self-compacting rubberised concrete (SCRC). *Constr. Build. Mater.* **2010**, *24*, 2043–2051. [CrossRef]
3. Raffoul, S.; Garcia, R.; Pilakoutas, K.; Guadagnini, M.; Medina, N.F. Optimisation of rubberised concrete with high rubber content: An experimental investigation. *Constr. Build. Mater.* **2016**, *124*, 391–404. [CrossRef]
4. Rezaifar, O.; Hasanzadeh, M.; Gholhaki, M. Concrete made with hybrid blends of crumb rubber and metakaolin: Optimization using Response Surface Method. *Constr. Build. Mater.* **2016**, *123*, 59–68. [CrossRef]
5. Fawzia, S.; Zhao, X.; Al-Mahaidi, R.; Rizkalla, S. Investigation into the bond between CFRP and steel tubes. In *FRP Composites in Civil Engineering-CICE 2004, Proceedings of the 2nd International Conference on FRP Composites in Civil Engineering, Adelaide, Australia, 8–10 December 2004*; Taylor and Francis: Oxford, UK, 2004.
6. Tafsirojjaman, T.; Fawzia, S.; Thambiratnam, D.; Zhao, X. Seismic strengthening of rigid steel frame with CFRP. *Arch. Civ. Mech. Eng.* **2019**, *19*, 334–347. [CrossRef]
7. Colombi, P.; Poggi, C. An experimental, analytical and numerical study of the static behavior of steel beams reinforced by pultruded CFRP strips. *Compos. Part B Eng.* **2006**, *37*, 64–73. [CrossRef]

8. George, J.M.; Kimiaei, M.; Elchalakani, M.; Fawzia, S. Experimental and numerical investigation of underwater composite repair with fibre reinforced polymers in corroded tubular offshore structural members under concentric and and ecentric axial loads. *Eng. Struct.* **2021**, *227*, 111402. [CrossRef]
9. Zeng, J.; Guo, Y.; Li, L.; Chen, W. Behavior and Three-Dimensional Finite Element Modeling of Circular Concrete Columns Partially Wrapped with FRP Strips. *Polymers* **2018**, *10*, 253. [CrossRef]
10. Nasrin, S.; Ibrahim, A. Numerical study on the low-velocity impact response of ultra-high-performance fiber reinforced concrete beams. *Structures* **2019**, *20*, 570–580. [CrossRef]
11. Zhang, B.; Teng, J.G.; Yu, T. Compressive Behavior of Double-Skin Tubular Columns with High-Strength Concrete and a Filament-Wound FRP Tube. *J. Compos. Constr.* **2017**, *21*, 04017029. [CrossRef]
12. Duarte, A.; Silva, B.; Silvestre, N.; de Brito, J.; Júlio, E.; Castro, J. Finite element modelling of short steel tubes filled with rubberized concrete. *Compos. Struct.* **2016**, *150*, 28–40. [CrossRef]
13. Duarte, A.; Silva, B.; Silvestre, N.; de Brito, J.; Júlio, E.; Castro, J. Tests and design of short steel tubes filled with rubberised concrete. *Eng. Struct.* **2016**, *112*, 274–286. [CrossRef]
14. Silva, A.; Jiang, Y.; Castro, J.; Silvestre, N.; Monteiro, R. Monotonic and cyclic flexural behaviour of square/rectangular rubberized concrete-filled steel tubes. *J. Constr. Steel Res.* **2017**, *139*, 385–396. [CrossRef]
15. Youssf, O.; ElGawady, M.A.; Mills, J.E.; Ma, X. An experimental investigation of crumb rubber concrete confined by fibre reinforced polymer tubes. *Constr. Build. Mater.* **2014**, *53*, 522–532. [CrossRef]
16. Khusru, S.; Fawzia, S.; Thambiratnam, D.P.; Elchalakani, M. A parametric study: High performance double skin tubular column using rubberised concrete. *Compos. Struct.* **2020**, *235*, 111741. [CrossRef]
17. Ayough, P.; Ibrahim, Z.; Sulong, N.R.; Hsiao, P.-C.; Elchalakani, M. Numerical analysis of square concrete-filled double skin steel tubular columns with rubberized concrete. *Structures* **2021**, *32*, 1026–1047. [CrossRef]
18. Youssf, O.; Hassanli, R.; Mills, J.E.; Zhuge, Y. Axial compression behaviour of hybrid double-skin tubular columns filled with rubcrete. *J. Compos. Sci.* **2019**, *3*, 62. [CrossRef]
19. Khusru, S.; Thambiratnam, D.P.; Elchalakani, M.; Fawzia, S. Experimental testing of novel hybrid rubberised concrete double skin tubular columns with filament wound CFRP tube under axial compressive loading. *Compos. Struct.* **2021**, *276*, 114568. [CrossRef]
20. Mander, J.B.; Priestley, M.J.N.; Park, R. Theoretical stress-strain model for confined concrete. *J. Struct. Eng.* **1988**, *114*, 1804–1826. [CrossRef]
21. De Maio, U.; Gaetano, D.; Greco, F.; Lonetti, P.; Pranno, A. The damage effect on the dynamic characteristics of FRP-strengthened reinforced concrete structures. *Compos. Struct.* **2023**, *309*, 116731. [CrossRef]
22. De Maio, U.; Gaetano, D.; Greco, F.; Lonetti, P.; Blasi, P.N.; Pranno, A. The Reinforcing Effect of Nano-Modified Epoxy Resin on the Failure Behavior of FRP-Plated RC Structures. *Buildings* **2023**, *13*, 1139. [CrossRef]
23. Chen, J.; Zhao, C.; Ding, F.; Xiang, P. Experimental study on the seismic behavior of precast concrete column with grouted corrugated sleeves and debonded longitudinal reinforcements. *Adv. Struct. Eng.* **2019**, *22*, 3277–3289. [CrossRef]
24. Li, Y.; Zhao, X.; Raman, R.S. Mechanical properties of seawater and sea sand concrete-filled FRP tubes in artificial seawater. *Constr. Build. Mater.* **2018**, *191*, 977–993. [CrossRef]
25. Manual ASUs. *The Abaqus Software Is a Product of Dassault Systèmes Simulia Corp*, Version 6; Dassault Systèmes: Providence, RI, USA, 2014.
26. Tao, Z.; Han, L.-H.; Zhao, X.-L. Behaviour of concrete-filled double skin (CHS inner and CHS outer) steel tubular stub columns and beam-columns. *J. Constr. Steel Res.* **2004**, *60*, 1129–1158. [CrossRef]
27. Hashin, Z.; Rotem, A. A fatigue failure criterion for fiber reinforced materials. *J. Compos. Mater.* **1973**, *7*, 448–464. [CrossRef]
28. Toh, W.; Bin Tan, L.; Tse, K.M.; Giam, A.; Raju, K.; Lee, H.P.; Tan, V.B.C. Material characterization of filament-wound composite pipes. *Compos. Struct.* **2018**, *206*, 474–483. [CrossRef]
29. Yu, T.; Teng, J.; Wong, Y.; Dong, S. Finite element modeling of confined concrete-II: Plastic-damage model. *Eng. Struct.* **2010**, *32*, 680–691. [CrossRef]
30. Lubliner, J.; Oliver, J.; Oller, S.; Onate, E. A plastic-damage model for concrete. *Int. J. Solids Struct.* **1989**, *25*, 299–326. [CrossRef]
31. Hibbitt, H.; Karlsson, B.; Sorensen, P. *Abaqus Analysis User's Manual Version 6*; Dassault Systèmes Simulia Corp: Providence, RI, USA, 2011.
32. Hany, N.F.; Hantouche, E.G.; Harajli, M.H. Finite element modeling of FRP-confined concrete using modified concrete damaged plasticity. *Eng. Struct.* **2016**, *125*, 1–14. [CrossRef]
33. Papanikolaou, V.K.; Kappos, A.J. Confinement-sensitive plasticity constitutive model for concrete in triaxial compression. *Int. J. Solids Struct.* **2007**, *44*, 7021–7048. [CrossRef]
34. Bompa, D.; Elghazouli, A. Stress–strain response and practical design expressions for FRP-confined recycled tyre rubber concrete. *Constr. Build. Mater.* **2020**, *237*, 117633. [CrossRef]
35. Han, L.-H.; Li, Y.-J.; Liao, F.-Y. Concrete-filled double skin steel tubular (CFDST) columns subjected to long-term sustained loading. *Thin-Walled Struct.* **2011**, *49*, 1534–1543. [CrossRef]
36. Pagoulatou, M.; Sheehan, T.; Dai, X.; Lam, D. Finite element analysis on the capacity of circular concrete-filled double-skin steel tubular (CFDST) stub columns. *Eng. Struct.* **2014**, *72*, 102–112. [CrossRef]
37. Lam, L.; Teng, J.G. Design-Oriented Stress-Strain Model for FRP-Confined Concrete in Rectangular Columns. *J. Reinf. Plast. Compos.* **2003**, *22*, 1149–1186. [CrossRef]

38. Li, Y.; Zhao, X.; Singh, R.R.; Al-Saadi, S. Experimental study on seawater and sea sand concrete filled GFRP and stainless steel tubular stub columns. *Thin-Walled Struct.* **2016**, *106*, 390–406. [CrossRef]
39. Teng, J.G.; Jiang, T.; Lam, L.; Luo, Y.Z. Refinement of a Design-Oriented Stress–Strain Model for FRP-Confined Concrete. *J. Compos. Constr.* **2009**, *13*, 269–278. [CrossRef]
40. Yu, T.; Wong, Y.; Teng, J. Behavior of hybrid FRP-concrete-steel double-skin tubular columns subjected to eccentric Compression. *Adv. Struct. Eng.* **2010**, *13*, 961–974. [CrossRef]